Monthly Notices of the ROYAL ASTRONOMICAL SOCIETY

MNRAS **434,** 59–68 (2013) doi:10.1093/mnras/stt968
Advance Access publication 2013 July 9

A statistical study on the low-frequency quasi-periodic oscillation amplitude spectrum and amplitude in GRS 1915+105

Shu-Ping Yan,[1,2]★ Guo-Qiang Ding,[1] Na Wang,[1]★ Jin-Lu Qu[3] and Li-Ming Song[3]

[1] *Xinjiang Astronomical Observatory, Chinese Academy of Sciences, 150 Science 1-Street, Urumqi, Xinjiang 830011, China*
[2] *University of Chinese Academy of Sciences, 19A Yuquan road, Beijing 100049, China*
[3] *Key Laboratory for Particle Astrophysics, Institute of High Energy Physics, Chinese Academy of Sciences, 19B Yuquan Road, Beijing 100049, China*

Accepted 2013 June 3. Received 2013 June 3; in original form 2013 January 29

ABSTRACT

A statistical study was made on both the energy dependence of the low-frequency quasi-periodic oscillation (QPO) amplitude (LFQPO amplitude spectrum) and the LFQPO amplitude from all the *RXTE* observations of GRS 1915+105. Based on the two-branch correlation of the LFQPO frequency and the hardness ratio, the observations that were suitable for evaluating the LFQPO amplitude spectrum were divided into two groups. According to a comparison between the radio and X-ray emissions, we deduced that the jets during the two groups of observations are very different. A negative correlation between the LFQPO frequency and the radio flux was found for one group. The LFQPO amplitude spectrum was fitted by a power law with an exponential cutoff in order to describe it quantitatively. It reveals that as the LFQPO frequency increases, the power law hardens. Furthermore, the cutoff energy first decreases, and then smoothly levels off. The fit also shows that the LFQPO amplitude spectra of the two groups are essentially the same, suggesting that the LFQPO does not originate from the jet. The LFQPO amplitude spectra are hard, indicating a possible origin of the LFQPO in the corona. As the LFQPO frequency increases, the LFQPO amplitude first increases and then decreases. The effects of the low-pass filter and the jet on the LFQPO amplitude are discussed.

Key words: accretion, accretion discs – black hole physics – X-rays: binaries – X-rays: individual: GRS 1915+105.

1 INTRODUCTION

The black hole binary system (BHB) GRS 1915+105 was discovered in 1992 with WATCH onboard *GRANAT* (Castro-Tirado, Brandt & Lund 1992). It is at a distance of ∼11 kpc (e.g. Fender et al. 1999; Zdziarski et al. 2005), and comprises a spinning black hole (Zhang, Cui & Chen 1997; McClintock et al. 2006) with mass $14 \pm 4\,M_{\odot}$, and a K–M III giant star with mass $0.8 \pm 0.5\,M_{\odot}$ as the donor (Harlaftis & Greiner 2004; Greiner et al. 2001b). The orbital separation of the binary components is about $108 \pm 4\,R_{\odot}$, and the orbital period is 33.5 ± 1.5 d (Greiner, Cuby & McCaughrean 2001a). GRS 1915+105 was the first microquasar to be found and produces superluminal radio jets (Mirabel & Rodríguez 1994; Fender et al. 1999).

It displays various X-ray light curves and complex timing phenomena. Based on the appearances of the light curves and colour-colour diagrams, the behaviours of GRS 1915+105 are classified into more than 10 categories (Belloni et al. 2000; Klein-Wolt et al. 2002; Hannikainen et al. 2005). These categories can be reduced to transitions among three basic states, namely states A, B and C. Three types of quasi-periodic oscillations (QPOs) with different QPO frequency bands have been observed in GRS 1915+105 (e.g. Morgan, Remillard & Greiner 1997; Chen, Swank & Taam 1997; Strohmayer 2001; Belloni, Méndez & Sánchez-Fernández 2001; Belloni et al. 2006). The low-frequency (∼0.5–10 Hz) QPO (LFQPO) is the type most commonly observed. Considerable effort has been put into exploring the origin of the LFQPO of GRS 1915+105. It has been shown that the LFQPO frequency is positively correlated with the fluxes of the thermal and power-law components as well as with the total flux (e.g. Chen et al. 1997; Markwardt, Swank & Taam 1999; Muno, Morgan & Remillard 1999; Trudolyubov, Churazov & Gilfanov 1999; Reig et al. 2000; Tomsick & Kaaret 2001; Muno et al. 2001). Muno et al. (1999) and Rodriguez et al. (2002b) reported that as the LFQPO frequency increases, the temperature of the inner accretion disc increases, and the disc radius decreases. These results indicate that the LFQPO is related to both the accretion disc and the region where the hard component is produced, for example the corona. It should be noted, however, that most of these results are dependent on spectral models, but the origin of the hard spectral component is still a matter of debate (e.g. Muno, Morgan & Remillard 1999; Rau & Greiner 2003; Vadawale et al.

★ E-mail: yanshup@xao.ac.cn (SPY); na.wang@xao.ac.cn (NW)

2003; Zdziarski et al. 2005; Titarchuk & Seifina 2009; Van Oers et al. 2010; Neilsen, Remillard & Lee 2011).

As model-independent approaches, it is useful to study the LFQPO frequency–LFQPO amplitude relation, the energy dependence of the LFQPO frequency (LFQPO frequency spectrum), and the energy dependence of the LFQPO amplitude (LFQPO amplitude spectrum) for GRS 1915+105. The LFQPO amplitude refers to the LFQPO fractional rms amplitude, which is measured by using a Lorentzian fit to the power spectrum (see Section 2 for details). It was found that the LFQPO amplitude is inversely correlated with the LFQPO frequency (e.g. Muno et al. 1999; Trudolyubov et al. 1999; Reig et al. 2000). Qu et al. (2010) studied the LFQPO frequency spectrum of GRS 1915+105 and found that as the centroid frequency of the LFQPO increases, the relation between LFQPO frequency and photon energy evolves from a negative correlation to a positive one. Three additional combined patterns of the negative correlation and the positive one have been discovered (Yan et al. 2012). Furthermore, as photon energy increases, the LFQPO amplitude increases and then flattens in some cases (e.g. Tomsick & Kaaret 2001; Rodriguez et al. 2002a, 2004; Zdziarski et al. 2005; Sobolewska & Życki 2006), indicating a possible association between the LFQPO and the corona (e.g. Morgan et al. 1997; Ingram & Done 2012).

There is no statistical study, however, in which all the *RXTE* observations of GRS 1915+105 on both the LFQPO amplitude spectrum and the LFQPO amplitude are utilized. In order to reveal more details of the LFQPO phenomenology and to investigate the origin of the LFQPO, in this study we analysed all the *RXTE*/PCA data of GRS 1915+105 and found that as the LFQPO frequency increases, the LFQPO amplitude spectrum becomes harder, and the LFQPO frequency–amplitude relation evolves smoothly from a positive correlation to a negative one. A negative correlation between the LFQPO frequency and the radio flux is also found. The observations and data reduction methods are described in Section 2, the results are presented in Section 3, and a discussion and the conclusions are given in Section 4.

2 OBSERVATIONS AND DATA REDUCTION

We searched the LFQPOs from all the *RXTE*/PCA observations of GRS 1915+105. Only some observations are suitable for evaluating the LFQPO amplitude spectrum. The LFQPO frequency sometimes varies obviously during an observation. In order to obtain credible results, this kind of observation is split into several time intervals during which the LFQPO frequency is relatively stable. A total of 168 observation intervals during which the X-ray emission is relatively hard and steady were obtained (Table 1).

It is a common technique to combine the timing analysis with the spectral analysis. In view of the debate over the spectral model, we investigate the relation between the hardness ratio (HR) and the LFQPO frequency as an approximate spectral analysis. The HR is defined as the ratio of the count rate in 7–60 keV to that in 2–7 keV. The corresponding PCA absolute channel intervals of the two energy bands in PCA gain epochs 3, 4 and 5 are 19–255 and 0–18, 16–255 and 0–15, and 17–255 and 0–16, respectively. The count rate is obtained by extracting the background-subtracted PCA Standard-2 light curve using the HEASOFT version 6.7 package.

In order to investigate the LFQPO amplitude spectrum, the light curves are extracted from the binned and event mode data. Good time intervals are defined as follows: a satellite elevation over the Earth limb $>10^\circ$ and an offset pointing $<0\overset{\circ}{.}02$. In order to acquire the details of the LFQPO amplitude spectrum with high enough confidence, only the binned mode data with energy channel number ≥ 4 and time resolution ≤ 8 ms are selected. The light curves are extracted with a time resolution of 8 ms in PCA energy bands defined in Table S1 in the Supporting Information. The power density spectra (PDSs) are computed with a 64-s sampling duration, with the normalization of Miyamoto et al. (1992), which gives the periodogram in units of $(\mathrm{rms/mean})^2\,\mathrm{Hz}^{-1}$. The Poisson noise is also corrected (e.g. van der Klis 1989; Vaughan et al. 2003). Following Belloni, Psaltis & van der Klis (2002), we fit the PDS with a model that includes several Lorentzians to represent the LFQPOs, the continuum and other broad features, respectively. The uncorrected LFQPO amplitude is defined as A_{raw} (per cent rms) $= 100 \times \sqrt{WN\pi/2}$, where W is the full width at half-maximum (FWHM) of the Lorentzian that represents the LFQPO, and N is the Miyamoto normalization of the Lorentzian. The LFQPO amplitude is further corrected for background (Berger & van der Klis 1994; Rodriguez & Varnière 2011). The errors are derived by varying the parameters until $\Delta\chi^2 = 1$ at the 1σ level.

In order to study the LFQPO frequency–amplitude relation, the light curves are extracted from the binned mode data in PCA absolute channel 0–35 (∼2–13 keV) and the event mode data in channel 36–255 (∼13–60 keV) with a time resolution of 8 ms. With the asynchronous rows deleted from the FITS files, the binned and event mode light curves in the same observation interval are added together to obtain a light curve that is used to measure the LFQPO frequency and amplitude.

3 RESULTS

3.1 LFQPO frequency–hardness ratio relationship

Fig. 1 shows the relationship between the LFQPO frequency and the HR. It can be seen that the points in this figure form two obviously separated branches. In order to clearly describe and analyse the results, we refer to the lower branch as ‘Branch 1’ (filled circles) and to the upper branch as ‘Branch 2’ (crosses), and divide the observation intervals into two groups corresponding to the two branches, respectively. Branch 1 is in the range ∼0.4–8 Hz, and Branch 2 is in the range ∼2–5.5 Hz. For Branch 1, as the LFQPO frequency increases, the HR first decreases, then smoothly levels off, and then increases slightly. For Branch 2, the HR decreases monotonically.

3.2 Spectral states of the Branch 1 and Branch 2 observations

Muno et al. (2001) investigated the radio and X-ray properties of GRS 1915+105 when its X-ray emission was hard and steady, and defined three spectral states/conditions. The energy spectra of the Branch 1 and Branch 2 observations are different based on the two-branch correlation of the LFQPO frequency and the HR. Thus, it is useful to identify the spectral states of the Branch 1 and Branch 2 observations. In order to clarify the states of the two groups of observations, we plot the *RXTE*/ASM count rate and the radio flux from the Ryle Telescope at 15.2 GHz as functions of time, and show the times of the observations analysed in this work (Figs 2a and b). The values of the radio flux were obtained from Muno et al. (2001). At first glance, the Branch 1 observations are in the time intervals (B1s in Fig. 2a) during which GRS 1915+105 produces the brightest radio emissions, and the Branch 2 observations are in the time intervals (B2s in Fig. 2a) when GRS 1915+105 produces fainter radio emissions.

The LFQPO frequency and amplitude as functions of time are also presented. The behaviour of the LFQPO frequency is similar

Table 1. List of GRS 1915+105 Observations suitable for evaluating the LFQPO amplitude spectrum.

					LFQPO			LFQPO amplitude spectrum[c]			
ObsID	Date	GTI[a] (s)	Count rate (cts/s/PCU2)	ChID[b]	Frequency (Hz)	Amplitude (per cent rms)	χ^2	α	E_c[d] (keV)	χ^2	Branch[e]
10258-01-02-00	29/07/96	9160	1739	Ch1E3	0.697 ± 0.002	10.8 ± 0.4	2.01	−0.39 ± 0.06	No cutoff	1.05	B_1
10258-01-03-00a	06/08/96	3328	1757	Ch1E3	1.687 ± 0.005	12.5 ± 0.5	2.65	−0.51 ± 0.03	49.6 ± 5.6	0.17	B_1
10258-01-03-00b	06/08/96	3360	1771	Ch1E3	1.332 ± 0.003	12.4 ± 0.7	2.18	−0.39 ± 0.03	81.3 ± 17.2	0.15	B_1
10258-01-03-00c	06/08/96	3360	1736	Ch1E3	1.453 ± 0.003	12.5 ± 0.5	2.25	−0.50 ± 0.07	54.9 ± 16.5	0.77	B_1
10258-01-04-00a	14/08/96	6800	1915	Ch1E3	2.694 ± 0.003	12.7 ± 0.2	3.13	−0.58 ± 0.04	45.3 ± 7.8	1.44	B_1
10258-01-04-00b	14/08/96	3408	1971	Ch1E3	3.133 ± 0.007	12.1 ± 0.3	2.18	−0.61 ± 0.06	48.8 ± 13.2	1.41	B_1
10258-01-05-00a	20/08/96	2688	3743	Ch2E3	6.370 ± 0.030	5.4 ± 0.2	1.74	−1.19 ± 0.22	18.4 ± 6.1	1.29	B_1
10258-01-05-00b	20/08/96	3376	3750	Ch2E3	6.359 ± 0.024	5.3 ± 0.2	2.22	−1.20 ± 0.20	19.5 ± 5.6	0.64	B_1
10258-01-06-00a	29/08/96	1400	5549	Ch2E3	7.338 ± 0.038	2.4 ± 0.2	1.22	−0.84 ± 0.26	No cutoff	2.00	B_1
10258-01-06-00b	29/08/96	3408	5587	Ch2E3	7.560 ± 0.024	2.2 ± 0.1	1.80	−1.08 ± 0.28	32.3 ± 23.1	2.77	B_1
10408-01-22-00	11/07/96	3328	2122	Ch2E3	3.476 ± 0.005	10.2 ± 0.3	1.03	−0.78 ± 0.05	30.1 ± 3.5	0.49	B_1
10408-01-22-01	11/07/96	3312	2020	Ch2E3	2.780 ± 0.005	11.9 ± 0.3	1.61	−0.69 ± 0.06	34.0 ± 5.4	0.96	B_1
10408-01-22-02a	11/07/96	1600	1989	Ch2E3	2.547 ± 0.008	12.0 ± 0.5	1.67	−0.74 ± 0.04	31.7 ± 3.2	0.20	B_1
10408-01-22-02b	11/07/96	820	1954	Ch2E3	2.509 ± 0.008	12.0 ± 0.8	1.79	−0.89 ± 0.02	22.6 ± 1.0	0.03	B_1
10408-01-22-02c	11/07/96	892	1929	Ch2E3	2.623 ± 0.009	11.8 ± 0.6	1.56	−0.74 ± 0.03	33.0 ± 2.2	0.05	B_1
10408-01-23-00a	14/07/96	3167	2109	Ch2E3	3.501 ± 0.006	11.2 ± 0.3	1.66	−0.71 ± 0.02	33.2 ± 1.8	0.14	B_1
10408-01-23-00b	14/07/96	3312	2108	Ch2E3	3.611 ± 0.005	11.0 ± 0.3	2.02	−0.74 ± 0.02	31.9 ± 2.0	0.19	B_1
10408-01-23-00c	14/07/96	3257	2255	Ch2E3	4.178 ± 0.008	10.3 ± 0.3	1.51	−0.69 ± 0.03	36.7 ± 3.8	0.34	B_1
10408-01-24-00a	16/07/96	2447	1949	Ch2E3	2.242 ± 0.006	12.7 ± 0.5	2.88	−0.58 ± 0.02	45.5 ± 3.9	0.11	B_1
10408-01-24-00b	16/07/96	3312	1943	Ch2E3	2.324 ± 0.005	13.2 ± 0.4	2.44	−0.69 ± 0.02	30.6 ± 1.5	0.11	B_1
10408-01-24-00c	16/07/96	2953	1952	Ch2E3	2.541 ± 0.004	12.2 ± 0.4	2.61	−0.59 ± 0.06	44.5 ± 9.3	0.75	B_1
10408-01-24-00d	16/07/96	913	1965	Ch2E3	2.597 ± 0.007	12.0 ± 0.7	1.65	−0.61 ± 0.05	44.2 ± 7.6	0.19	B_1
10408-01-25-00	19/07/96	9952	1820	Ch1E3	1.130 ± 0.002	12.7 ± 0.3	2.46	−0.47 ± 0.04	65.0 ± 14.1	0.80	B_1
10408-01-27-00a	26/07/96	2336	1783	Ch1E3	0.645 ± 0.002	10.6 ± 0.9	1.42	−0.55 ± 0.11	63.2 ± 26.3	0.15	B_1
10408-01-27-00b	26/07/96	3296	1791	Ch1E3	0.618 ± 0.002	9.3 ± 0.7	1.07	−0.53 ± 0.05	57.0 ± 11.7	0.15	B_1
10408-01-27-00c	26/07/96	3296	1769	Ch1E3	0.629 ± 0.003	9.7 ± 0.6	1.28	−0.41 ± 0.04	79.5 ± 19.4	0.11	B_1
10408-01-28-00a	03/08/96	3328	1742	Ch1E3	0.996 ± 0.002	11.8 ± 0.6	1.61	−0.40 ± 0.05	93.8 ± 36.2	0.30	B_1
10408-01-28-00b	03/08/96	3328	1744	Ch1E3	0.964 ± 0.004	11.2 ± 0.6	1.13	−0.36 ± 0.05	No cutoff	0.28	B_1
10408-01-28-00c	03/08/96	3328	1731	Ch1E3	0.926 ± 0.002	12.2 ± 0.6	1.49	−0.34 ± 0.05	No cutoff	0.37	B_1
10408-01-29-00a	10/08/96	2965	1760	Ch1E3	1.664 ± 0.003	12.3 ± 0.5	1.64	−0.55 ± 0.05	51.9 ± 11.0	0.43	B_1
10408-01-29-00b	10/08/96	3392	1784	Ch1E3	1.857 ± 0.004	12.3 ± 0.6	1.73	−0.57 ± 0.05	65.0 ± 15.4	0.37	B_1
10408-01-29-00c	10/08/96	3392	1787	Ch1E3	1.954 ± 0.004	12.4 ± 0.5	1.56	−0.53 ± 0.07	52.4 ± 16.2	0.93	B_1
10408-01-30-00a	18/08/96	1696	2388	Ch1E3	4.316 ± 0.013	9.3 ± 0.3	1.64	−0.82 ± 0.04	29.2 ± 3.0	0.23	B_1
10408-01-30-00b	18/08/96	1696	2588	Ch1E3	4.794 ± 0.012	8.1 ± 0.3	1.29	−0.71 ± 0.03	42.4 ± 6.4	0.14	B_1
10408-01-30-00c	18/08/96	1696	2842	Ch1E3	5.204 ± 0.017	7.1 ± 0.3	1.40	−0.86 ± 0.10	23.8 ± 6.2	0.83	B_1
10408-01-30-00d	18/08/96	1696	2752	Ch1E3	4.902 ± 0.012	7.4 ± 0.4	1.07	−0.79 ± 0.04	31.4 ± 3.6	0.15	B_1
10408-01-30-00e	18/08/96	1688	2986	Ch1E3	5.431 ± 0.014	5.5 ± 0.3	1.15	−0.64 ± 0.07	54.6 ± 20.8	0.36	B_1
10408-01-31-00a	25/08/96	2319	2327	Ch1E3	4.101 ± 0.006	9.5 ± 0.3	1.72	−0.76 ± 0.08	36.2 ± 9.8	1.33	B_1
10408-01-31-00b	25/08/96	1000	2555	Ch1E3	4.672 ± 0.014	8.0 ± 0.4	1.32	−0.87 ± 0.09	21.6 ± 4.4	0.55	B_1
10408-01-31-00c	25/08/96	1328	2496	Ch1E3	4.487 ± 0.014	8.5 ± 0.3	1.49	−0.94 ± 0.08	18.7 ± 2.9	0.77	B_1
10408-01-31-00d	25/08/96	1000	2323	Ch1E3	4.172 ± 0.012	9.4 ± 0.4	2.06	−0.82 ± 0.05	30.6 ± 4.2	0.29	B_1
10408-01-31-00e	25/08/96	1664	2133	Ch1E3	3.632 ± 0.008	10.3 ± 0.4	1.39	−0.75 ± 0.06	36.2 ± 6.5	0.51	B_1
10408-01-31-00f	25/08/96	1664	2057	Ch1E3	3.388 ± 0.007	10.8 ± 0.4	1.69	−0.82 ± 0.05	26.4 ± 3.0	0.31	B_1
10408-01-32-00a	31/08/96	2912	4239	Ch1E3	6.654 ± 0.033	3.2 ± 0.2	2.25	−1.25 ± 0.33	24.2 ± 17.7	6.35	B_1
10408-01-32-00b	31/08/96	3312	3648	Ch1E3	5.965 ± 0.019	4.4 ± 0.2	2.38	−1.09 ± 0.15	20.4 ± 6.7	1.82	B_1
10408-01-32-00c	31/08/96	1170	3314	Ch1E3	5.674 ± 0.029	5.4 ± 0.3	1.60	−0.93 ± 0.03	30.4 ± 3.7	0.02	B_1
10408-01-33-00a	07/09/96	912	3527	Ch1E3	5.610 ± 0.034	5.3 ± 0.3	1.67	−0.63 ± 0.12	No cutoff	0.52	B_1
10408-01-33-00b	07/09/96	2495	3743	Ch1E3	5.708 ± 0.022	4.3 ± 0.2	1.79	−1.04 ± 0.19	25.2 ± 11.7	2.43	B_1
10408-01-33-00c	07/09/96	1295	3655	Ch1E3	5.542 ± 0.040	5.0 ± 0.3	1.91	−0.77 ± 0.09	No cutoff	2.75	B_1
10408-01-42-00a	23/10/96	3312	3289	Ch1E3	5.063 ± 0.010	5.6 ± 0.2	2.44	−0.80 ± 0.09	23.7 ± 5.1	1.09	B_2
10408-01-42-00b	23/10/96	3312	2921	Ch1E3	4.709 ± 0.010	6.6 ± 0.2	2.20	−0.57 ± 0.08	No cutoff	0.76	B_2
10408-01-43-00a	23/10/96	2416	3274	Ch1E3	5.020 ± 0.011	5.7 ± 0.2	1.85	−1.02 ± 0.10	17.3 ± 3.3	0.56	B_2
10408-01-43-00b	23/10/96	2284	3314	Ch1E3	5.077 ± 0.013	5.6 ± 0.2	2.01	−0.60 ± 0.20	No cutoff	2.84	B_2
10408-01-43-00c	23/10/96	1980	3302	Ch1E3	5.135 ± 0.013	5.5 ± 0.2	1.67	−0.70 ± 0.12	27.6 ± 9.6	0.89	B_2
10408-01-43-00d	23/10/96	1740	2709	Ch1E3	4.462 ± 0.014	7.2 ± 0.3	1.91	−0.74 ± 0.12	33.1 ± 12.9	1.02	B_2
20186-03-02-052a	17/09/97	3031	3096	Ch3E3	5.390 ± 0.016	5.3 ± 0.3	1.56	−1.12 ± 0.07	17.1 ± 2.1	0.38	B_1
20186-03-02-052b	17/09/97	3031	3203	Ch3E3	5.818 ± 0.019	5.9 ± 0.2	1.95	−1.05 ± 0.14	25.5 ± 11.0	1.20	B_1
20186-03-02-052c	17/09/97	3312	2348	Ch3E3	4.086 ± 0.006	9.3 ± 0.2	1.34	−1.00 ± 0.06	21.4 ± 2.5	1.46	B_1
20186-03-02-052d	17/09/97	3312	2563	Ch3E3	4.634 ± 0.008	8.2 ± 0.2	1.16	−1.06 ± 0.06	18.6 ± 2.2	1.29	B_1
20186-03-02-052e	17/09/97	3312	2802	Ch3E3	5.157 ± 0.011	6.5 ± 0.2	1.43	−1.01 ± 0.06	20.5 ± 2.8	0.81	B_1
20186-03-02-060a	18/09/97	2768	2852	Ch3E3	4.984 ± 0.022	7.6 ± 0.3	1.00	−0.81 ± 0.08	42.9 ± 16.8	0.75	B_1
20186-03-02-060b	18/09/97	9936	4385	Ch3E3	6.761 ± 0.036	4.7 ± 0.1	1.55	−0.71 ± 0.03	No cutoff	1.34	B_1

Table 1 – *continued*

ObsID	Date	GTI[a] (s)	Count rate (cts/s/PCU2)	ChID[b]	LFQPO Frequency (Hz)	LFQPO Amplitude (per cent rms)	LFQPO χ^2	LFQPO amplitude spectrum[c] α	LFQPO amplitude spectrum[c] E_c[d] (keV)	LFQPO amplitude spectrum[c] χ^2	Branch[e]
20186-03-02-060c	18/09/97	3312	2679	Ch3E3	4.788 ± 0.011	7.9 ± 0.2	1.33	−0.87 ± 0.05	31.7 ± 5.3	0.62	B_1
20186-03-02-06a	18/09/97	1656	2767	Ch3E3	5.042 ± 0.017	7.3 ± 0.2	1.17	−0.97 ± 0.12	24.0 ± 6.5	1.66	B_1
20186-03-02-06b	18/09/97	1656	2430	Ch3E3	4.240 ± 0.012	8.5 ± 0.3	1.50	−0.86 ± 0.05	28.4 ± 4.3	0.67	B_1
20186-03-02-06c	18/09/97	1600	2255	Ch3E3	3.820 ± 0.009	10.0 ± 0.4	1.42	−1.02 ± 0.04	18.9 ± 1.4	0.40	B_1
20186-03-02-06d	18/09/97	1695	2399	Ch3E3	4.291 ± 0.009	9.0 ± 0.3	1.38	−1.07 ± 0.07	18.5 ± 2.6	0.86	B_1
20186-03-02-06e	18/09/97	1550	2761	Ch3E3	5.060 ± 0.014	7.0 ± 0.3	1.28	−1.01 ± 0.11	21.7 ± 5.6	1.06	B_1
20186-03-02-06f	18/09/97	1569	3648	Ch3E3	5.949 ± 0.060	6.1 ± 0.3	1.32	−0.72 ± 0.13	No cutoff	0.79	B_1
20402-01-05-00	05/12/96	2048	1421	Ch5E3	2.819 ± 0.004	13.2 ± 0.3	1.38	−0.82 ± 0.10	21.9 ± 4.3	8.10	B_2
20402-01-06-00a	11/12/96	3312	1360	Ch5E3	3.032 ± 0.009	12.7 ± 0.5	1.13	−0.87 ± 0.10	19.8 ± 3.7	2.68	B_2
20402-01-06-00b	11/12/96	3312	1279	Ch5E3	2.837 ± 0.007	13.2 ± 0.5	1.23	−0.74 ± 0.07	25.2 ± 4.0	2.03	B_2
20402-01-06-00c	11/12/96	2780	1211	Ch5E3	2.569 ± 0.007	13.0 ± 0.5	1.40	−0.78 ± 0.09	25.0 ± 4.8	2.46	B_2
20402-01-07-00	19/12/96	9296	1310	Ch5E3	3.116 ± 0.005	13.0 ± 0.2	1.78	−0.89 ± 0.07	17.4 ± 2.4	4.31	B_2
20402-01-08-00a	24/12/96	2658	1318	Ch5E3	3.859 ± 0.010	10.7 ± 0.3	1.52	−0.81 ± 0.09	20.7 ± 4.5	1.22	B_2
20402-01-08-00b	24/12/96	2834	1325	Ch5E3	3.934 ± 0.010	10.6 ± 0.3	2.26	−0.87 ± 0.08	18.6 ± 3.3	1.23	B_2
20402-01-08-01	25/12/96	3312	1232	Ch5E3	3.469 ± 0.009	12.0 ± 0.3	1.35	−0.72 ± 0.10	28.6 ± 8.3	2.45	B_2
20402-01-09-00	31/12/96	7548	1099	Ch5E3	2.816 ± 0.006	12.9 ± 0.3	1.77	−0.73 ± 0.08	23.4 ± 4.4	4.50	B_2
20402-01-10-00	08/01/97	9804	993	Ch5E3	2.912 ± 0.006	12.6 ± 0.2	2.07	−0.77 ± 0.08	22.2 ± 3.7	5.10	B_2
20402-01-11-00	14/01/97	6519	912	Ch5E3	2.919 ± 0.007	11.7 ± 0.3	1.53	−0.84 ± 0.11	19.7 ± 4.0	4.46	B_2
20402-01-12-00a	23/01/97	5695	883	Ch5E3	2.802 ± 0.006	12.1 ± 0.4	1.37	−0.76 ± 0.07	23.0 ± 3.2	1.34	B_2
20402-01-12-00b	23/01/97	3755	894	Ch5E3	2.783 ± 0.007	11.7 ± 0.5	1.50	−0.75 ± 0.11	23.9 ± 6.2	1.83	B_2
20402-01-13-00	29/01/97	10000	936	Ch5E3	3.650 ± 0.007	11.7 ± 0.2	2.02	−0.82 ± 0.15	20.5 ± 6.5	13.4	B_2
20402-01-14-00	01/02/97	9394	910	Ch5E3	3.566 ± 0.007	11.6 ± 0.2	2.00	−0.82 ± 0.10	19.9 ± 4.1	5.31	B_2
20402-01-15-00	09/02/97	10222	816	Ch5E3	2.260 ± 0.004	12.2 ± 0.3	1.71	−0.55 ± 0.08	37.3 ± 9.8	4.15	B_2
20402-01-16-00	22/02/97	5951	803	Ch5E3	2.977 ± 0.007	11.1 ± 0.3	1.21	−0.62 ± 0.06	28.4 ± 4.8	1.31	B_2
20402-01-20-00	17/03/97	7300	807	Ch5E3	3.208 ± 0.006	11.1 ± 0.3	1.43	−0.75 ± 0.13	24.1 ± 7.5	5.50	B_2
20402-01-26-00a	25/04/97	2220	1137	Ch5E3	3.959 ± 0.012	10.6 ± 0.3	1.76	−0.92 ± 0.10	16.2 ± 2.7	1.17	B_2
20402-01-26-00b	25/04/97	2884	1188	Ch5E3	4.286 ± 0.010	10.3 ± 0.3	2.08	−0.97 ± 0.10	15.5 ± 2.7	1.07	B_2
20402-01-26-00c	25/04/97	3300	1210	Ch5E3	4.468 ± 0.016	10.0 ± 0.3	1.94	−0.93 ± 0.14	21.0 ± 6.1	2.30	B_2
20402-01-26-00d	25/04/97	3328	1178	Ch5E3	4.258 ± 0.017	9.7 ± 0.3	1.74	−0.69 ± 0.14	41.3 ± 23.3	2.46	B_2
20402-01-26-00e	25/04/97	1964	1163	Ch5E3	4.391 ± 0.014	9.9 ± 0.3	2.08	−0.83 ± 0.10	21.4 ± 4.8	1.04	B_2
20402-01-48-00a	29/09/97	3296	4714	Ch5E3	7.589 ± 0.036	2.6 ± 0.1	1.56	−0.96 ± 0.08	No cutoff	1.39	B_1
20402-01-48-00b	29/09/97	3328	2726	Ch5E3	4.712 ± 0.014	6.7 ± 0.3	1.60	−0.95 ± 0.07	24.5 ± 4.6	0.60	B_1
20402-01-50-01	16/10/97	4994	1497	Ch5E3	1.047 ± 0.003	11.0 ± 0.5	2.16	−0.57 ± 0.03	45.6 ± 4.8	0.25	B_1
20402-01-51-00	22/10/97	9399	1490	Ch5E3	1.396 ± 0.002	12.6 ± 0.3	3.30	−0.57 ± 0.03	50.4 ± 5.7	0.73	B_1
30182-01-01-00	08/07/98	11606	1435	Ch3E3	2.139 ± 0.003	15.6 ± 0.3	2.09	−0.73 ± 0.06	31.5 ± 5.2	5.23	B_2
30182-01-02-00a	09/07/98	5073	1889	Ch3E3	3.248 ± 0.005	12.7 ± 0.3	1.57	−0.89 ± 0.08	22.0 ± 3.7	4.96	B_2
30182-01-02-00b	09/07/98	3359	2069	Ch3E3	3.544 ± 0.006	11.9 ± 0.3	1.55	−0.89 ± 0.09	21.7 ± 3.9	4.17	B_2
30182-01-02-00c	09/07/98	2968	2466	Ch3E3	3.975 ± 0.008	9.9 ± 0.3	1.73	−0.90 ± 0.07	21.0 ± 2.9	1.48	B_2
30182-01-03-00a	10/07/98	3344	3479	Ch3E3	5.097 ± 0.014	5.7 ± 0.2	2.54	−0.93 ± 0.06	25.3 ± 3.6	0.36	B_2
30182-01-03-00b	10/07/98	2472	3677	Ch3E3	5.166 ± 0.011	5.0 ± 0.2	1.91	−0.78 ± 0.07	29.1 ± 6.4	0.45	B_2
30182-01-04-00a	11/07/98	1678	2360	Ch3E3	4.110 ± 0.010	9.2 ± 0.3	1.54	−1.04 ± 0.10	18.3 ± 3.4	1.93	B_2
30182-01-04-00b	11/07/98	4166	1933	Ch3E3	3.403 ± 0.006	11.5 ± 0.3	1.65	−1.03 ± 0.08	18.5 ± 2.5	3.99	B_2
30182-01-04-00c	11/07/98	3328	1709	Ch3E3	2.918 ± 0.005	12.3 ± 0.4	1.86	−0.97 ± 0.08	20.5 ± 3.1	3.39	B_2
30182-01-04-00d	11/07/98	3324	1604	Ch3E3	2.665 ± 0.005	13.3 ± 0.4	1.63	−0.89 ± 0.09	23.4 ± 4.3	3.77	B_2
30182-01-04-01a	12/07/98	2236	1581	Ch3E3	2.641 ± 0.006	13.6 ± 0.7	1.03	−0.87 ± 0.09	21.8 ± 4.1	2.26	B_2
30182-01-04-01b	12/07/98	2728	1513	Ch3E3	2.411 ± 0.005	14.4 ± 0.5	1.45	−0.83 ± 0.08	26.0 ± 4.7	2.31	B_2
30182-01-04-01c	12/07/98	3340	1605	Ch3E3	2.723 ± 0.006	13.9 ± 0.4	1.18	−0.83 ± 0.08	26.2 ± 4.8	3.31	B_2
30182-01-04-01d	12/07/98	3340	2010	Ch3E3	3.377 ± 0.013	13.5 ± 0.3	1.44	−0.89 ± 0.11	20.4 ± 4.2	4.72	B_2
30182-01-04-01e	12/07/98	2400	2665	Ch3E3	4.222 ± 0.010	8.5 ± 0.3	2.13	−0.85 ± 0.10	21.9 ± 4.7	1.94	B_2
30402-01-09-01	10/04/98	2546	1979	Ch6E3	2.157 ± 0.004	12.9 ± 0.4	2.44	−0.68 ± 0.04	31.0 ± 3.7	0.72	B_1
30402-01-10-00a	11/04/98	3312	1970	Ch6E3	1.590 ± 0.003	12.8 ± 0.6	1.14	−0.60 ± 0.04	41.3 ± 6.4	0.60	B_1
30402-01-10-00b	11/04/98	6303	1956	Ch6E3	1.722 ± 0.003	12.7 ± 0.3	3.77	−0.60 ± 0.03	40.3 ± 4.6	0.79	B_1
30402-01-11-00a	20/04/98	3311	2777	Ch6E3	5.401 ± 0.013	7.5 ± 0.2	2.42	−0.87 ± 0.09	22.5 ± 4.8	1.15	B_1
30402-01-11-00b	20/04/98	2271	2952	Ch6E3	5.827 ± 0.018	6.9 ± 0.2	1.74	−0.80 ± 0.13	26.6 ± 10.2	1.57	B_1
30703-01-16-00	28/04/98	5038	1816	Ch6E3	1.376 ± 0.003	12.6 ± 0.4	1.40	−0.65 ± 0.05	33.1 ± 4.9	1.41	B_1
30703-01-17-00	06/05/98	4584	1739	Ch6E3	0.926 ± 0.002	11.8 ± 0.5	1.67	−0.51 ± 0.05	48.9 ± 9.3	0.68	B_1
30703-01-22-00	27/06/98	3375	1539	Ch6E3	2.253 ± 0.005	14.2 ± 0.5	1.98	−0.73 ± 0.03	31.7 ± 3.1	0.60	B_2
30703-01-25-00a	23/07/98	2626	1718	Ch6E3	3.175 ± 0.007	12.6 ± 0.4	1.21	−0.90 ± 0.11	20.9 ± 4.2	4.66	B_2
30703-01-25-00b	23/07/98	2322	2146	Ch6E3	3.810 ± 0.009	10.3 ± 0.3	1.31	−0.90 ± 0.10	18.5 ± 3.5	2.36	B_2
30703-01-33-00	15/09/98	4917	1400	Ch6E3	3.297 ± 0.007	12.5 ± 0.3	1.21	−0.82 ± 0.09	20.3 ± 3.5	4.40	B_2
30703-01-41-00	26/12/98	4707	1233	Ch6E3	2.154 ± 0.004	14.8 ± 0.4	1.59	−0.59 ± 0.05	38.9 ± 7.0	1.69	B_2
40403-01-08-00	02/06/99	9884	1584	Ch6E4	2.475 ± 0.003	13.6 ± 0.3	3.25	−0.72 ± 0.06	34.3 ± 5.5	4.39	B_2

Table 1 – *continued*

					LFQPO			LFQPO amplitude spectrum[c]			
ObsID	Date	GTI[a] (s)	Count rate (cts/s/PCU2)	ChID[b]	Frequency (Hz)	Amplitude (per cent rms)	χ^2	α	E_c[d] (keV)	χ^2	Branch[e]
40403-01-09-00	08/07/99	13355	1343	Ch6E4	2.030 ± 0.003	15.6 ± 0.3	2.08	−0.66 ± 0.08	39.9 ± 10.0	9.89	B_2
40403-01-11-00	28/02/00	13355	2426	Ch6E4	4.339 ± 0.010	8.0 ± 0.3	2.38	−0.68 ± 0.09	34.5 ± 10.9	1.41	B_2
40703-01-01-00	01/01/99	9731	1281	Ch6E4	2.264 ± 0.003	15.0 ± 0.3	1.88	−0.69 ± 0.07	29.2 ± 5.1	4.92	B_2
40703-01-02-00	08/01/99	9005	1861	Ch6E4	3.568 ± 0.005	11.5 ± 0.2	1.80	−0.72 ± 0.08	27.8 ± 6.3	7.23	B_2
40703-01-05-00	12/02/99	10129	1592	Ch6E4	4.204 ± 0.006	10.0 ± 0.1	2.51	−0.85 ± 0.09	19.7 ± 3.5	5.77	B_2
40703-01-09-00	28/03/99	4702	1418	Ch6E4	2.782 ± 0.005	12.9 ± 0.3	1.11	−0.76 ± 0.08	24.9 ± 4.2	2.67	B_2
40703-01-38-02	15/11/99	2501	5138	Ch6E4	7.978 ± 0.036	2.9 ± 0.1	1.12	−0.94 ± 0.04	No cutoff	0.45	B_1
50125-01-01-03	13/07/00	2735	1747	Ch3E5	3.021 ± 0.006	13.0 ± 0.4	1.62	−0.73 ± 0.07	35.0 ± 7.2	2.29	B_2
50125-01-03-00a	15/07/00	4348	2077	Ch3E5	3.548 ± 0.007	12.1 ± 0.3	1.64	−0.80 ± 0.07	27.3 ± 4.6	3.26	B_2
50125-01-03-00b	15/07/00	10652	1818	Ch3E5	3.184 ± 0.004	12.9 ± 0.2	3.25	−0.81 ± 0.07	26.7 ± 4.2	7.47	B_2
50703-01-01-00	08/03/00	4755	1314	Ch6E4	2.343 ± 0.007	15.9 ± 0.5	1.22	−0.61 ± 0.07	31.6 ± 6.4	2.15	B_2
50703-01-49-00	27/02/01	5467	1434	Ch6E5	2.611 ± 0.004	13.2 ± 0.3	2.19	−0.85 ± 0.10	27.0 ± 6.2	5.46	B_2
50703-01-55-01	17/04/01	6896	1583	Ch6E5	2.839 ± 0.004	13.8 ± 0.3	2.00	−0.70 ± 0.09	34.5 ± 9.3	8.04	B_2
50703-01-67-00	22/07/01	1806	1243	Ch6E5	2.183 ± 0.005	14.6 ± 0.8	1.33	−0.65 ± 0.07	41.7 ± 9.9	1.16	B_2
60100-01-01-00	05/08/01	3280	1249	Ch6E5	2.225 ± 0.004	14.3 ± 0.6	1.42	−0.60 ± 0.09	50.6 ± 18.7	2.63	B_2
60100-01-02-000a	06/08/01	2748	1487	Ch6E5	2.712 ± 0.005	14.6 ± 0.5	1.29	−0.60 ± 0.08	34.0 ± 8.6	2.86	B_2
60100-01-02-000b	06/08/01	2496	1654	Ch6E5	3.017 ± 0.006	13.5 ± 0.5	1.11	−0.58 ± 0.11	40.2 ± 16.0	3.84	B_2
60100-01-02-000c	06/08/01	2648	1762	Ch6E5	3.201 ± 0.007	12.9 ± 0.4	1.47	−0.75 ± 0.10	23.2 ± 5.3	3.36	B_2
60100-01-02-000d	06/08/01	2816	1967	Ch6E5	3.516 ± 0.007	11.3 ± 0.3	1.38	−0.61 ± 0.11	43.9 ± 21.5	4.36	B_2
60100-01-02-000e	06/08/01	2964	2178	Ch6E5	3.845 ± 0.009	10.1 ± 0.3	2.28	−0.72 ± 0.06	27.2 ± 4.7	1.10	B_2
60405-01-03-00	05/08/01	6560	1474	Ch6E5	2.729 ± 0.004	14.3 ± 0.3	1.56	−0.66 ± 0.09	29.8 ± 7.3	5.78	B_2
60701-01-16-00	28/02/02	3068	1820	Ch6E5	0.377 ± 0.002	7.6 ± 0.6	0.73	−0.35 ± 0.05	No cutoff	0.17	B_1
60701-01-16-01	28/02/02	3109	1809	Ch6E5	0.395 ± 0.002	8.3 ± 0.9	1.02	−0.45 ± 0.11	50.2 ± 29.3	0.21	B_1
60701-01-23-00	22/01/02	3263	1986	Ch6E5	2.073 ± 0.003	13.0 ± 0.4	2.92	−0.82 ± 0.05	21.7 ± 2.5	0.42	B_1
60701-01-28-00	06/03/02	9680	1744	Ch6E5	0.466 ± 0.001	9.0 ± 0.5	1.49	−0.31 ± 0.04	No cutoff	0.40	B_1
60701-01-33-00	24/04/02	3247	1426	Ch6E5	1.029 ± 0.002	10.8 ± 0.6	1.09	−0.46 ± 0.07	99.0 ± 59.0	0.91	B_1
70702-01-23-00	03/10/02	3231	1931	Ch6E5	3.449 ± 0.005	12.1 ± 0.4	1.54	−0.69 ± 0.13	28.3 ± 9.5	3.98	B_2
70702-01-24-00	09/10/02	3264	1328	Ch6E5	2.581 ± 0.005	12.9 ± 0.5	2.51	−0.74 ± 0.10	41.6 ± 13.8	2.86	B_2
70703-01-01-08	01/04/02	10704	1902	Ch3E5	2.589 ± 0.004	11.7 ± 0.2	4.27	−0.69 ± 0.07	34.1 ± 7.3	3.56	B_1
70703-01-01-14	29/03/02	8240	1869	Ch6E5	2.634 ± 0.004	12.6 ± 0.2	4.02	−0.65 ± 0.03	37.3 ± 4.4	1.21	B_1
80127-02-03-00	10/04/03	11728	1884	Ch4E5	1.088 ± 0.002	13.3 ± 0.4	2.18	−0.40 ± 0.05	97.9 ± 38.1	2.64	B_1
80701-01-08-00	25/10/06	3216	2375	Ch6E5	4.652 ± 0.012	8.0 ± 0.2	1.51	−0.97 ± 0.13	20.2 ± 5.5	1.57	B_2
80701-01-26-00	28/11/06	6304	1334	Ch6E5	2.543 ± 0.003	14.2 ± 0.4	2.24	−0.75 ± 0.08	25.2 ± 4.8	1.99	B_2
80701-01-32-00	04/12/06	6239	1212	Ch6E5	2.102 ± 0.003	15.6 ± 0.5	1.75	−0.49 ± 0.09	41.7 ± 12.6	5.33	B_2
80701-01-51-00	09/12/06	6960	1252	Ch6E5	2.222 ± 0.003	15.0 ± 0.4	1.91	−0.58 ± 0.07	39.0 ± 9.7	2.99	B_2
80701-01-55-02	11/01/07	5440	1131	Ch6E5	2.609 ± 0.003	14.4 ± 0.4	1.87	−0.60 ± 0.10	30.0 ± 8.3	6.07	B_2
80701-01-56-00	18/01/07	9600	1073	Ch6E5	2.557 ± 0.002	13.2 ± 0.3	3.58	−0.68 ± 0.08	47.6 ± 14.5	4.03	B_2
80701-01-57-00	24/01/07	9584	1100	Ch6E5	2.063 ± 0.004	13.6 ± 0.4	3.49	−0.43 ± 0.06	72.9 ± 25.9	2.68	B_2
90105-01-03-01	15/05/04	7152	3023	Ch4E5	4.944 ± 0.009	7.1 ± 0.2	1.82	−0.77 ± 0.09	34.7 ± 10.9	2.42	B_1
90105-07-01-00	12/04/05	6464	2098	Ch4E5	4.018 ± 0.005	10.4 ± 0.2	1.62	−0.82 ± 0.05	21.4 ± 2.3	0.95	B_1
90105-07-02-00	13/04/05	6368	2123	Ch4E5	3.890 ± 0.006	11.1 ± 0.2	1.99	−0.87 ± 0.07	18.8 ± 2.6	1.88	B_1
90701-01-19-00	28/07/04	6416	1200	Ch6E5	2.116 ± 0.002	14.5 ± 0.4	1.89	−0.66 ± 0.07	41.5 ± 9.2	3.05	B_2
91701-01-55-00	02/05/07	9584	1091	Ch6E5	1.986 ± 0.003	15.1 ± 0.6	2.69	−0.47 ± 0.07	74.9 ± 25.5	0.94	B_2
92702-01-09-00	04/05/06	5136	1071	Ch6E5	3.817 ± 0.005	11.5 ± 0.2	1.31	−0.99 ± 0.11	14.2 ± 2.4	1.62	B_2

[a]The lengths of the good time intervals.
[b]ChID represents the definition of PCA energy bands for the light curve extraction detailed in Table S1.
[c]The LFQPO amplitude spectrum is fitted by a power law with an exponential cutoff.
[d]No cutoff is detected in some observations at least up to ∼100 keV.
[e]In the LFQPO frequency–hardness diagram, the points follow two obviously separated branches, which are designated 'B_1' and 'B_2', respectively.

to the behaviour of the count rate (Fig. 2c). The LFQPO amplitude is, however, a non-monotonic function of the count rate (Fig. 2d).

In order to show the relationship between the radio emission and the LFQPO more clearly, we need to bin the observations into time intervals. The time intervals of the radio fluxes presented in Fig. 2 are about 1 d. We therefore select 1 d as the bin size. Fig. 3 shows the radio flux as a function of time, and the relationship between the radio flux and the LFQPO frequency. Obviously, most of the radio fluxes corresponding to Branch 1 observations are larger than 30 mJy, and all except one flux corresponding to Branch 2 observations are lower than 40 mJy. As shown in Fig. 3(b), for Branch 1, the LFQPO frequency is negatively correlated with the radio flux. For Branch 2, it has no obvious correlation with the radio flux. The points of Branch 1 in Fig. 3(b) are fitted using least squares. The slope of the best-fitting line is −0.047 ± 0.015 Hz mJy^{-1}, and the adjusted R^2 is 0.62.

The Branch 2 point whose radio flux is about 90 mJy is located at some distance from the main Branch 2 group. We therefore checked

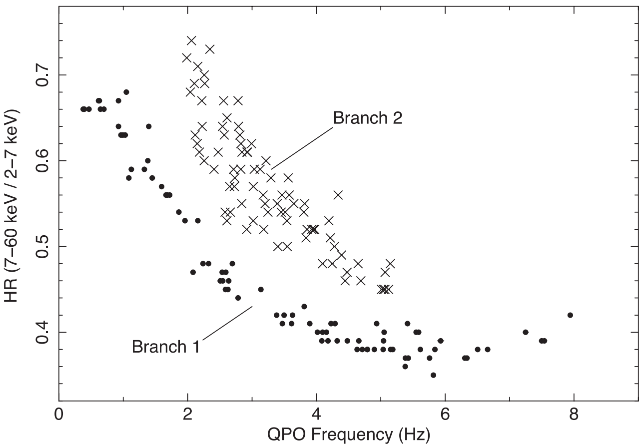

Figure 1. The hardness (HR) as a function of the LFQPO frequency. The points form two obviously separated branches, termed Branch 1 and Branch 2, respectively. The Branch 1 observations are marked with filled circles and the Branch 2 observations are marked with crosses, and similarly in subsequent figures.

it and found that its *RXTE* observation time was a bit earlier than its Ryle observation time, and that the radio flux on the days around this observation time was ∼20–30 mJy. It is thus possible that the radio flux corresponding to the *RXTE* observation is not actually so high, and the outlying Branch 2 point might actually be located within the main group. This is just speculation, however, owing to the lack of data. We also checked all the other radio fluxes and found that they are close to those on either side of them. These fluxes thus seem to be more reliable, although some uncertainty still exists. The states of the two group observations will be discussed in Section 4.

3.3 LFQPO amplitude spectrum

For each interval listed in Table 1, we have drawn a diagram to show the LFQPO amplitude spectrum. Although these spectra have various shapes, they evolve with the LFQPO frequency. Fig. 4 shows several representative spectra of the Branch 1 observations. When the LFQPO frequency is very low, the amplitude increases slightly with energy (Fig. 4a). As the LFQPO frequency increases, the amplitude in the higher energy band gradually increases (Figs 4b and c), and then the amplitudes in both the higher and lower energy bands gradually decrease (Fig. 4d and e). For the LFQPOs with higher frequency, however, the amplitude in the higher energy band is relatively high (Fig. 4e). Fig. 5 shows representative spectra of the Branch 2 observations. When the LFQPO frequency is low, the amplitude spectrum is steep (Fig. 5a). As the LFQPO frequency increases, the amplitude in the higher energy band decreases (Fig. 5b), and then the amplitudes in both the higher and lower energy bands decrease (Figs 5c and d).

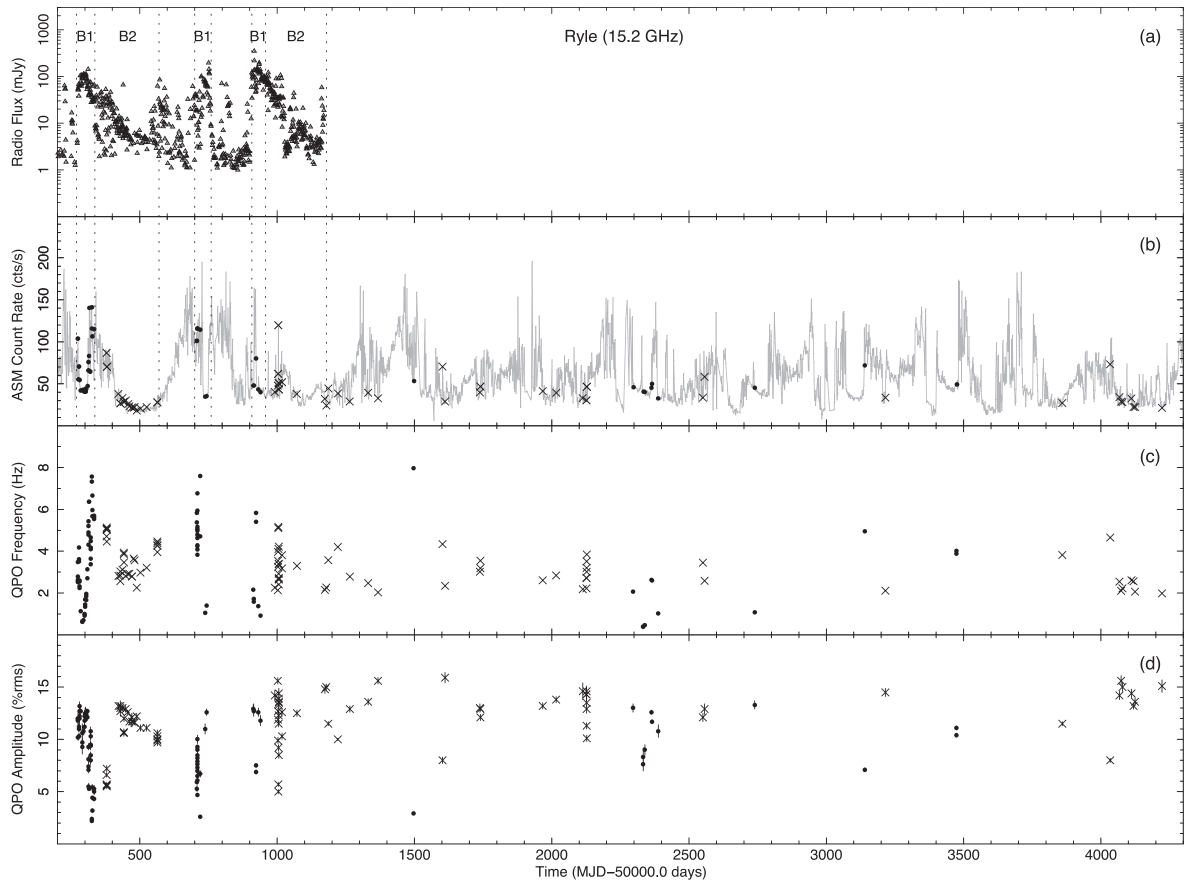

Figure 2. (a) Flux as a function of time from the Ryle Telescope at 15.2 GHz. The radio fluxes were obtained from fig. 1 in Muno et al. (2001). The vertical dotted lines are plotted to show clearly the radio conditions of the Branch 1 and Branch 2 observations. (b) The *RXTE*/ASM light curve (grey curve) and the observation times of the two groups of observations. The bin size is 1 d. The data were provided by the ASM/*RXTE* teams at MIT and at the *RXTE* Science Operations Facility and Guest Observer Facility at NASA's Goddard Space Flight Center. (c) The LFQPO frequency and (d) amplitude as functions of the time.

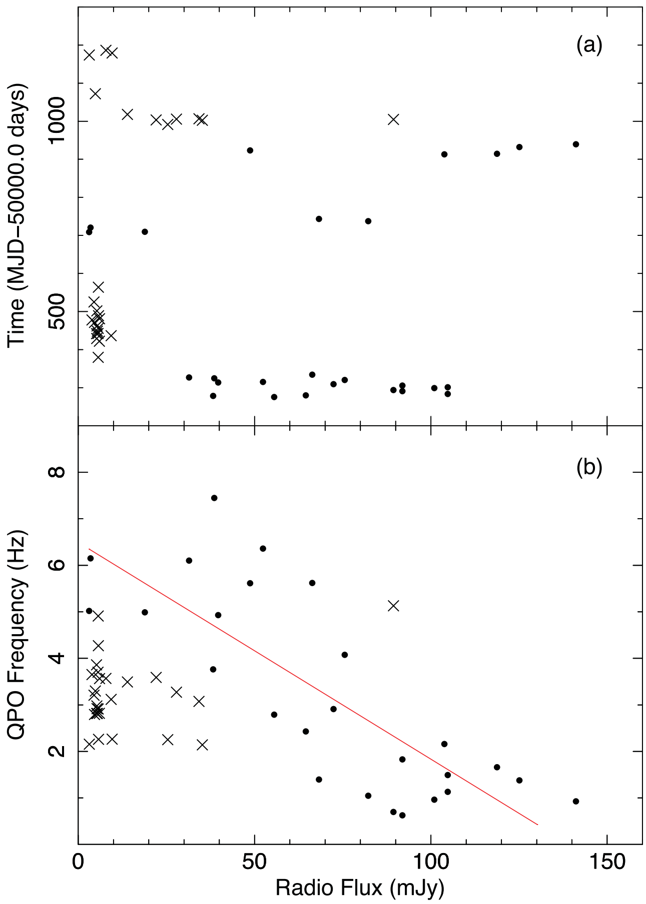

Figure 3. The observations shown in Fig. 2 are binned into time intervals. The bin size is 1 d. (a) Radio flux as a function of time. (b) The relationship between the radio flux and the LFQPO frequency.

In order to describe the LFQPO amplitude spectrum quantitatively, we fitted the spectrum by a power law with an exponential cutoff, $A(E) = KE^{-\alpha}\exp(-E/E_{\rm c})$, where α is the power-law index and $E_{\rm c}$ is the e-folding energy of exponential roll-off. Fig. 6 shows α and $E_{\rm c}$ as functions of the LFQPO frequency. Clearly, the two groups of points are essentially identical, indicating that there is not much difference between the two groups of observations in the LFQPO amplitude spectrum. Thus, the two groups of points will later be fitted as a whole. As the LFQPO frequency increases from ~0.4 to ~8 Hz, α decreases from ~−0.4 to ~−1.1. (Fig. 6a). The points are fitted using least squares. The slope of the best-fitting line is $-0.087 \pm 0.012\,{\rm Hz}^{-1}$, and the adjusted R^2 is 0.53. Fig. 6(b) presents the LFQPO frequency dependence of $E_{\rm c}$. At lower LFQPO frequencies, the dependence starts at an $E_{\rm c}$ of ~80 keV and follows a negative correlation until a certain LFQPO frequency, where it levels off. The points are fitted with the function $E(f) = A - D\,B\ln\{\exp[(f_{\rm tr} - f)/D] + 1\}$ (function (1) in Shaposhnikov & Titarchuk 2007). The best-fitting values are $A = 25.1 \pm 2.8$ keV, $B = -21.6 \pm 8.0\,{\rm Hz}^{-1}$, $D = 0.3 \pm 0.5$ Hz and $f_{\rm tr} = 2.84 \pm 0.55$ Hz. The errors for the best-fitting parameters are standard deviations.

3.4 LFQPO frequency–amplitude relationship

The relationship between the LFQPO frequency and amplitude is shown in Fig. 7. For Branch 1, as the LFQPO frequency increases, the LFQPO amplitude increases from ~7 to ~13 per cent at $f < 2$ Hz, and then decreases from ~13 to ~2 per cent at $f > 2$ Hz. For Branch 2, as the LFQPO frequency increases, the LFQPO amplitude decreases monotonically from ~16 to ~5 per cent.

The LFQPO absolute amplitude is estimated by multiplying the LFQPO amplitude by the corresponding count rate (see e.g. Méndez et al. 1997; Gilfanov, Revnivtsev & Molkov 2003; Zdziarski et al. 2005). For Branch 1, as the LFQPO frequency increases, the LFQPO amplitude increases at $f < 2$ Hz and then decreases, similar to the behaviour of the LFQPO amplitude. For Branch 2, the points are widely scattered (Fig. 8).

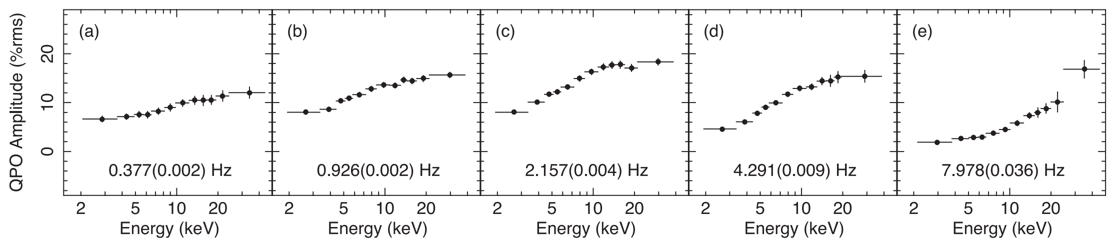

Figure 4. Representative LFQPO amplitude spectra of the Branch 1 observations. The observation IDs are (a) 60701-01-16-00, (b) 30703-01-17-00, (c) 30402-01-09-01, (d) 20186-03-02-06d, and (e) 40703-01-38-02. The frequencies shown are the LFQPO centroid frequencies. The horizontal bars denotes the width of the energy band. The vertical bars are error bars.

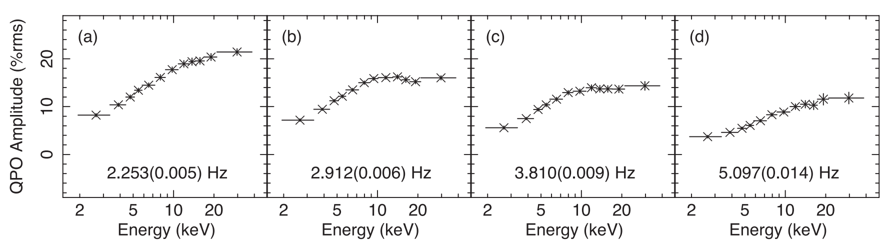

Figure 5. Representative LFQPO amplitude spectra of the Branch 2 observations. The observation IDs are (a) 30703-01-22-00, (b) 20402-01-10-00, (c) 30703-01-25-00b, and (d) 30182-01-03-00a. The frequencies shown are the LFQPO centroid frequencies. The horizontal bars denotes the width of the energy band. The vertical bars are error bars.

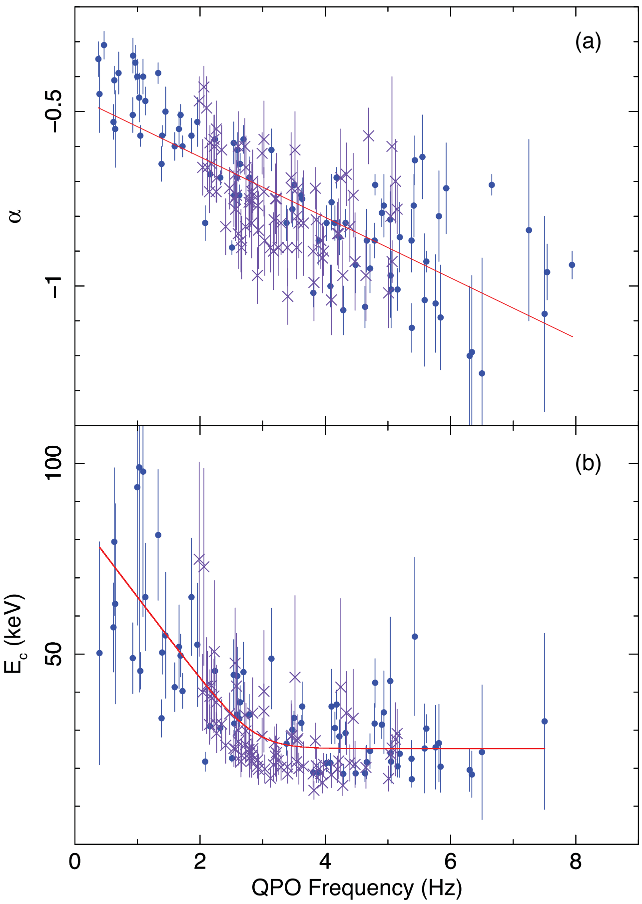

Figure 6. The LFQPO amplitude spectrum is fitted by a power law with an exponential cutoff. (a) The power-law index as a function of the LFQPO frequency. The points are fitted using least squares. (b) The cutoff energy as a function of the LFQPO frequency. The points are fitted with function (1) in Shaposhnikov & Titarchuk (2007).

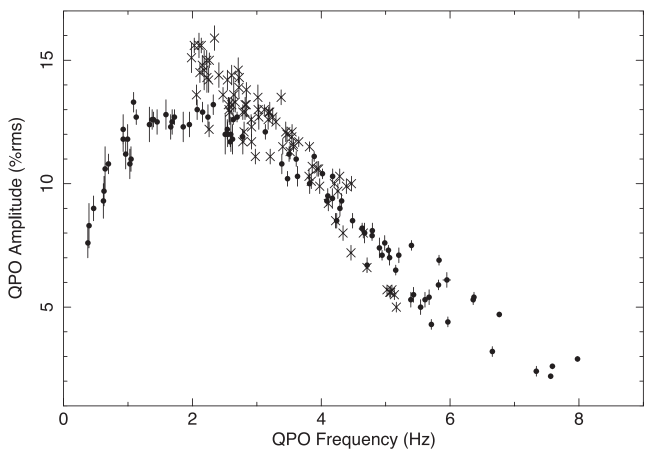

Figure 7. The relationship between the LFQPO frequency and the LFQPO fractional amplitude.

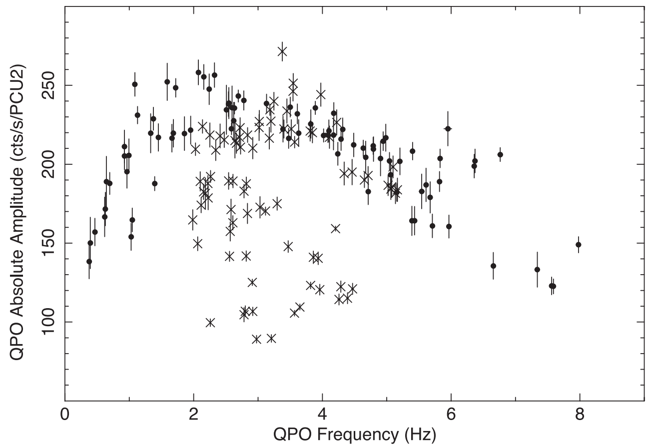

Figure 8. The relationship between the LFQPO frequency and the LFQPO absolute amplitude.

4 DISCUSSION AND CONCLUSIONS

LFQPOs have been detected in many BHBs (see e.g. van der Klis 2004; McClintock et al. 2006; Remillard & McClintock 2006). Their frequencies and amplitudes are usually correlated with spectral parameters of both the thermal and power-law components (e.g. Chen et al. 1997; Markwardt, Swank & Taam 1999; Muno, Morgan & Remillard 1999; Trudolyubov et al. 1999; Reig et al. 2000; Sobczak et al. 2000; Revnivtsev, Trudolyubov & Borozdin 2000; Tomsick & Kaaret 2001; Muno et al. 2001; Vignarca et al. 2003). However, neither the QPO mechanism (e.g. Stella & Vietri 1998; Stella, Vietri & Morsink 1999; Wagoner 1999; Tagger & Pellat 1999; Chakrabarti & Manickam 2000; Nobili et al. 2000; Titarchuk & Osherovich 2000; Psaltis & Norman 2000; Ingram, Done & Fragile 2009) nor the origin of the power-law component (see e.g. Done, Gierliński & Kubota 2007) is very clear. Thus, we have adopted a model-independent strategy to study the phenomenon of the LFQPOs.

Based on a statistical study of both the LFQPO amplitude spectrum and the LFQPO amplitude of GRS 1915+105, we find that in the LFQPO frequency–HR diagram the points form two branches, which are designated as Branch 1 and Branch 2 (Fig. 1). This indicates that the energy spectra of the observations corresponding to the two branches are very different. Similar phenomena have been found by other authors. For instance, Belloni et al. (2000) showed that the χ state points follow two branches in the colour-colour diagram and used different spectral models for the observations located on the two branches. Rau & Greiner (2003) studied four years of *RXTE* observations of GRS 1915+105 during the χ state and revealed a two-branch correlation of the power-law slope and the power-law normalization. Their two branches correspond to our Branch 1 and Branch 2. Van Oers et al. (2010) analysed two observations that belong to Branch 1 and Branch 2, respectively, and found that their best-fitting model parameters were significantly different.

Identifying the states of the Branch 1 and Branch 2 observations is helpful for analysing the properties and origin of the LFQPO. Muno et al. (2001) investigated the radio and X-ray properties of GRS 1915+105 when the X-ray emission was hard and steady, and established that radio emission always accompanies the hard state of GRS 1915+105, but that the radio flux and the X-ray flux are not correlated. They defined 'radio plateau conditions' (the radio flux at 15.2 GHz is >20 mJy and the radio spectrum is optically thick with power law $E^{-\alpha_{\rm r}}$, where $\alpha_{\rm r} < 0.2$), 'radio steep conditions' (the radio flux at 15.2 GHz is >20 mJy and the radio spectrum is optically thin with $\alpha_{\rm r} > 0.2$), and 'radio faint conditions' (the radio flux at 15.2 GHz is <20 mJy) for the hard-steady X-ray observations. The radio emission is generally believed to be synchrotron emission from ejected plasma in sporadic or continuous jets (e.g. Fender et al. 1995). For GRS 1915+105, the optically thick radio emission during plateau conditions has been resolved as a compact jet of relativistic electrons (Dhawan, Mirabel & Rodríguez 2000). The optically thin radio emission during steep conditions originates from material ejected from the central source (Mirabel & Rodríguez 1994; Fender et al. 1999; Dhawan et al. 2000). The radio-faint observations show some properties similar to a weak radio-plateau state. The radio-steep observations represent the transition into and out of radio-plateau conditions. As the LFQPO frequency decreases, the radio emission becomes brighter and optically thick. The source is in plateau conditions when the LFQPO frequency is lower than 2 Hz. By combining our results shown in Section 3.2 with the definitions and conclusions in the literature presented here, we deduce that for Branch 1, as the LFQPO frequency increases, the source evolves from radio-plateau conditions to radio-faint conditions via radio-steep conditions, and for Branch 2, the source is mainly in the radio-faint condition (Figs 2 and 3). It should be pointed out that the radio conditions of some observations cannot be identified owing to the lack of radio data. Nevertheless, the two branches are clearly separate and smoothly evolve in the LFQPO frequency–HR diagram, which reflects the smooth evolution of spectral state. Therefore, the lack of radio data has no effect on our identification of state.

Despite the significant difference between the spectral states of the Branch 1 and Branch 2 observations, and the fact that the radio emissions at a given LFQPO frequency are always stronger during Branch 1 observations than during Branch 2 observations (Fig. 3b), there is no essential difference between the LFQPO amplitude spectra of the two branches (Figs 4, 5 and 6). Thus, the LFQPO seems not to originate from the jet, as the jets of GRS 1915+105 during Branch 1 and Branch 2 observations are very different. The spectrum of the LFQPO amplitude is hard (Figs 4 and 5), suggesting that the LFQPO is related to the corona (e.g. Morgan et al. 1997; Ingram & Done 2012). Shaposhnikov & Titarchuk (2007) showed that as the LFQPO frequency increases, the spectral index of the X-ray spectrum, α_x, increases linearly and then smoothly levels off to become a constant. The α_x–LFQPO frequency relationship is fitted with function (1) in Shaposhnikov & Titarchuk (2007), and the obtained transition frequency is 2.23 ± 0.07 Hz. Coincidentally, we find that as the LFQPO frequency increases, E_c of the LFQPO amplitude spectrum also decreases and then smoothly levels off (Fig. 6b). The E_c–LFQPO frequency relationship is fitted with the same function, and the transition frequency is 2.84 ± 0.55 Hz. The similarity of the behaviours of the two correlations is another indication of the link between the LFQPO and the corona, although the details are as yet not very clear.

For Branch 1, the LFQPO amplitude increases with frequency until ∼2 Hz; above this, it decreases. Negative correlations between LFQPO amplitude and frequency have been observed in GRS 1915+105 and other BHBs (e.g. Muno et al. 1999; Sobczak et al. 2000; McClintock et al. 2009; Heil, Vaughan & Uttley 2011). The aperiodic variability also shows a decrease in amplitude above ∼ a few hertz (e.g. Pottschmidt et al. 2003; Axelsson, Borgonovo & Larsson 2005; Done et al. 2007; Kalemci et al. 2003, 2006). These negative correlations are often attributed to a low-pass filter acting to suppress variability above ∼2–5 Hz (e.g. Done et al. 2007; Gierliński, Nikołajuk & Czerny 2008; Heil et al. 2011). On the other hand, at $f \lesssim 2$ Hz, the decrease in the LFQPO amplitude coincides with the growth of the jet, indicating a possible correlation between them. If the jet emits X-rays, considering the decreases in both the LFQPO fractional and absolute amplitudes (Figs 7, 8 and 6b), the decrease of the LFQPO fractional amplitude might partly be attributable to the increase in the X-ray flux of the jet, which is independent of the LFQPO. Even if the jet does not emit X-rays, the decrease might be attributable to the weakening of the LFQPO itself owing to some sort of process, for example more accretion material/energy forms the jet but not the corona. Yan et al. (2013) also presented a decrease in the LFQPO amplitude that coincides with the possible production of a short-lived jet in GRS 1915+105. Thus our result tends to support the existence of a short-lived jet. Because the low-pass filter mainly suppresses variability above several hertz and the radio flux is inversely correlated with the LFQPO frequency, it might be that both the low-pass filter and the jet affect the LFQPO amplitude, and that the former plays a dominant role at $f \gtrsim 2$ Hz while the later plays a dominant role at $f \lesssim 2$ Hz. The word 'dominant' here refers only to the comparison between the effects of the low-pass filter and the jet.

If the LFQPO does come from the corona, then the negative correlation between the LFQPO frequency and the radio flux indicates a strong correlation between the corona and the jet. In the context of the truncated disc model, this means that decreasing the disc truncation radius leads to a higher QPO frequency (e.g. Done et al. 2007; Ingram et al. 2009) and a weaker jet.

For Branch 2, it is interesting to note that the points of the LFQPO absolute amplitude are distributed sporadically, while the points of the LFQPO amplitude are distributed regularly. More intriguingly, the LFQPO amplitude of Branch 2 is roughly in line with that of Branch 1 in the LFQPO amplitude–frequency relationship, hinting that a common mechanism, for example a low-pass filter, might work.

In summary, we have made a statistical study of both the LFQPO amplitude spectrum and amplitude in GRS 1915+105. The observations are divided into two groups based on the appearance of the LFQPO frequency–HR diagram. The jets of GRS 1915+105 during the two groups of observations are very different. For one group, the LFQPO frequency is negatively correlated with the radio flux. We fitted the LFQPO amplitude spectrum by a power law with a cutoff, and found that as the LFQPO frequency increases, the spectrum becomes harder. In addition, there is no significant difference between the two groups of observations in the LFQPO amplitude spectrum, indicating that the LFQPO does not originate from the jet. The LFQPO amplitude spectrum is hard, suggesting that the LFQPO originates from the corona. As the LFQPO frequency increases, the LFQPO frequency–amplitude relationship evolves from a positive correlation to a negative one, which might be a result of the combined effect of the low-pass filter and the jet on the LFQPO amplitude.

ACKNOWLEDGEMENTS

We thank the anonymous referee for comments that greatly improved the quality of the manuscript. We thank Ms Qian Yang for her help with the English. This research has made use of data obtained from the High Energy Astrophysics Science Archive Research Center (HEASARC), provided by NASA's Goddard Space Flight Center. This work is supported by CAS (KJCX2-YW-T09), 973 Program (2009CB824800), NSFC (11143013, 11173024, 11203063 and 11203064), and WLF of CAS (XBBS201123, LHXZ201201 and XBBS201121).

REFERENCES

Axelsson M., Borgonovo L., Larsson S., 2005, A&A, 438, 999
Belloni T., Klein-Wolt M., Méndez M., van der Klis M., van Paradijs J., 2000, A&A, 355, 271
Belloni T., Méndez M., Sánchez-Fernández C., 2001, A&A, 372, 551
Belloni T., Psaltis D., van der Klis M., 2002, ApJ, 572, 392
Belloni T., Soleri P., Casella P., Méndez M., Migliari S., 2006, MNRAS, 369, 305
Berger M., van der Klis M., 1994, A&A, 292, 175
Castro-Tirado A. J., Brandt S., Lund N., 1992, IAU Circ., 5590, 2
Chakrabarti S. K., Manickam S. G., 2000, ApJ, 531, L41
Chen X., Swank J. H., Taam R. E., 1997, ApJ, 477, L41
Dhawan V., Mirabel I. F., Rodríguez L. F., 2000, ApJ, 543, 373
Done C., Gierliński M., Kubota A., 2007, A&AR, 15, 1
Fender R. P., Bell Burnell S. J., Garrington S. T., Spencer R. E., Pooley G. G., 1995, MNRAS, 274, 633
Fender R. P., Garrington S. T., McKay D. J., Muxlow T. W. B., Pooley G. G., Spencer R. E., Stirling A. M., Waltman E. B., 1999, MNRAS, 304, 865
Gierliński M., Nikołajuk M., Czerny B., 2008, MNRAS, 383, 741
Gilfanov M., Revnivtsev M., Molkov S., 2003, A&A, 410, 217
Greiner J., Cuby J. G., McCaughrean M. J., 2001a, Nat, 414, 522
Greiner J., Cuby J. G., McCaughrean M. J., Castro-Tirado A. J., Mennickent R. E., 2001b, A&A, 373, L37
Hannikainen D. C. et al., 2005, A&A, 435, 995
Harlaftis E. T., Greiner J., 2004, A&A, 414, L13
Heil L. M., Vaughan S., Uttley P., 2011, MNRAS, 411, L66
Ingram A., Done C., 2012, MNRAS, 427, 934
Ingram A., Done C., Fragile P. C., 2009, MNRAS, 397, L101
Kalemci E., Tomsick J. A., Rothschild R. E., Pottschmidt K., Corbel S., Wijnands R., Miller J. M., Kaaret P., 2003, ApJ, 586, 419
Kalemci E., Tomsick J. A., Rothschild R. E., Pottschmidt K., Corbel S., Kaaret P., 2006, ApJ, 639, 340
Klein-Wolt M., Fender R. P., Pooley G. G., Belloni T., Migliari S., Morgan E. H., van der Klis M., 2002, MNRAS, 331, 745
van der Klis M., 1989, ARA&A, 27, 517
van der Klis M., 2004, preprint (arXiv:astro-ph/0410551)
McClintock J. E., Shafee R., Narayan R., Remillard R. A., Davis S. W., Li L.-X., 2006, ApJ, 652, 518
McClintock J. E., Remillard R. A., Rupen M. P., Torres M. A. P., Steeghs D., Levine A. M., Orosz J. A., 2009, ApJ, 698, 1398
Markwardt C. B., Swank J. H., Taam R. E., 1999, ApJ, 513, L37
Méndez M., van der Klis M., van Paradijs J., Lewin W. H. G., Lamb F. K., Vaughan B. A., Kuulkers E., Psaltis D., 1997, ApJ, 485, L37
Mirabel I. F., Rodríguez L. F., 1994, Nat, 371, 46
Miyamoto S., Kitamoto S., Iga S., Negoro H., Terada K., 1992, ApJ, 391, L21
Morgan E. H., Remillard R. A., Greiner J., 1997, ApJ, 482, 993
Muno M. P., Morgan E. H., Remillard R. A., 1999, ApJ, 527, 321
Muno M. P., Remillard R. A., Morgan E. H., Waltman E. B., Dhawan V., Hjellming R. M., Pooley G., 2001, ApJ, 556, 515
Neilsen J., Remillard R. A., Lee J. C., 2011, ApJ, 737, 69
Nobili L., Turolla R., Zampieri L., Belloni T., 2000, ApJ, 538, L137
Pottschmidt K. et al., 2003, A&A, 407, 1039
Psaltis D., Norman C., 2000, preprint (arXiv:astro-ph/0001391)
Qu J. L., Lu F. J., Lu Y., Song L. M., Zhang S., Ding G. Q., Wang J. M., 2010, ApJ, 710, 836
Rau A., Greiner J., 2003, A&A, 397, 711
Reig P., Belloni T., van der Klis M., Méndez M., Kylafis N. D., Ford E. C., 2000, ApJ, 541, 883
Remillard R. A., McClintock J. E., 2006, ARA&A, 44, 49
Revnivtsev M. G., Trudolyubov S. P., Borozdin K. N., 2000, MNRAS, 312, 151
Rodriguez J., Varnière P., 2011, ApJ, 735, 79
Rodriguez J., Durouchoux P., Mirabel I. F., Ueda Y., Tagger M., Yamaoka K., 2002a, A&A, 386, 271
Rodriguez J., Varnière P., Tagger M., Durouchoux P., 2002b, A&A, 387, 487
Rodriguez J., Corbel S., Hannikainen D. C., Belloni T., Paizis A., Vilhu O., 2004, ApJ, 615, 416
Shaposhnikov N., Titarchuk L., 2007, ApJ, 663, 445
Sobczak G. J., McClintock J. E., Remillard R. A., Cui W., Levine A. M., Morgan E. H., Orosz J. A., Bailyn C. D., 2000, ApJ, 531, 537
Sobolewska M. A., Życki P. T., 2006, MNRAS, 370, 405
Stella L., Vietri M., 1998, ApJ, 492, L59
Stella L., Vietri M., Morsink S. M., 1999, ApJ, 524, L63
Strohmayer T. E., 2001, ApJ, 554, L169
Tagger M., Pellat R., 1999, A&A, 349, 1003
Titarchuk L., Osherovich V., 2000, ApJ, 542, L111
Titarchuk L., Seifina E., 2009, ApJ, 706, 1463
Tomsick J. A., Kaaret P., 2001, ApJ, 548, 401
Trudolyubov S. P., Churazov E. M., Gilfanov M. R., 1999, Astron. Lett., 25, 718
Vadawale S. V., Rao A. R., Naik S., Yadav J. S., Ishwara-Chandra C. H., Pramesh Rao A., Pooley G. G., 2003, ApJ, 597, 1023
Van Oers P. et al., 2010, MNRAS, 409, 763
Vaughan S., Edelson R., Warwick R. S., Uttley P., 2003, MNRAS, 345, 1271
Vignarca F., Migliari S., Belloni T., Psaltis D., van der Klis M., 2003, A&A, 397, 729
Wagoner R. V., 1999, Phys. Rep., 311, 259
Yan S.-P. et al., 2012, Ap&SS, 337, 137
Yan S.-P., Wang N., Ding G.-Q., Qu J.-L., 2013, ApJ, 767, 44
Zdziarski A. A., Gierliński M., Rao A. R., Vadawale S. V., Mikołajewska J., 2005, MNRAS, 360, 825
Zhang S. N., Cui W., Chen W., 1997, ApJ, 482, L155

SUPPORTING INFORMATION

Additional Supporting Information may be found in the online version of this article:

Table 1. The definitions of *RXTE*/PCA energy bands for light curve extraction (http://mnras.oxfordjournals.org/lookup/suppl/doi:10.1093/mnras/stt968/-/DC1).

Please note: Oxford University Press are not responsible for the content or functionality of any supporting materials supplied by the authors. Any queries (other than missing material) should be directed to the corresponding author for the article.

This paper has been typeset from a TEX/LATEX file prepared by the author.